Periodica Polytechnica
Transportation Engineering

47(1), pp. 6-12, 2019
https://doi.org/10.3311/PPtr.11562

RESEARCH ARTICLE

Design of Shaft Respecting the Fatigue Limit for Ultra-High Number of Cycles

Otakar Bokůvka[1], Michal Jambor[1*], Slavomír Hrček[2], Ján Šteininger[2], František Nový[1], Libor Trško[3]

Received 02 April 2017; accepted 05 October 2017

Abstract

Advances in engineering solutions in recent few decades caused that conventional fatigue limit (for steels and cast irons given for number of 10^7 cycles) is no more sufficient. Construction parts of newly introduced transport vehicles, operating at high velocities and at long distances, reach during their lifetime very high numbers of loading cycles, in order of 10^9. For this reason, values of fatigue limits for 10^9 cycles must be considered in design and construction of transport vehicles. In this study, authors present how dramatically will change the design of shaft, when fatigue limit for 10^9 cycles is considered.

Keywords

Shaft design, ADI cast iron, ultra-high cycle fatigue, mechanical design

[1] Department of Materials Engineering,
Faculty of Mechanical Engineering,
University of Žilina, Univerzitná 8215/1,
010 26 Žilina, Slovak Republic

[2] Department of Design and Mechanical Elements,
Faculty of Mechanical Engineering,
University of Žilina, Univerzitná 8215/1,
010 26 Žilina, Slovak Republic

[3] Research Centre of University of Žilina
University of Žilina, Univerzitná 8215/1,
010 26 Žilina, Slovak Republic

[*] Corresponding author, e-mail: michal.jambor@fstroj.uniza.sk

1 Introduction

Continuous progress and advances in technological solutions especially in the field of transportation, reveals new problems related to the designing of structural parts mainly cyclical loaded components as shafts and wheels which are, during their life, loaded by very high number of cycles (>10^7). This number exceeds conventionally defined numbers of cycles for fatigue strength (for steels usually 10^7 cycles) and therefore these conventional determined values are insufficient in design components loaded by the very high number of cycles. Research in this field has shown that in metal materials fatigue strength decrease continuously with increasing number of loading cycles even behind, in past sufficient, 10^7 cycles. In this context term "gigacycle fatigue" was introduced, which represent an area of cyclic loading in the range from 10^7 to 10^{10} cycles. As it's shown in the recent researches, some different mechanisms can take place in this area of cyclic loading, especially in the stage of crack initiation, which can lead to the continuous decrease of fatigue strength when the structural components are cyclically loaded by very high numbers of cycles. For this reason, is necessary to know values of fatigues strength in gigacycle region, if designing components are intended to be cyclically loaded in this region (Murakami, 2002; Bokůvka et al., 2015; Bathias, 1999; Ritchie, 1999; Stanzl, 1999).

As an experimental material was used ADI cast iron, representing widespread material for manufacturing shafts, wheels and other cyclically loaded components of transport machines. ADI cast iron provide excellent combination of properties as high tensile strength, yield strength, hardness and wear resistance while retaining sufficient toughness and ductility and good technological properties. ADI cast iron is produced by isothermal heat treatment of ductile iron, which is alloyed with Cu, Mo and Ni, as these elements modify TTT diagrams and it allows achieving an unique microstructure after heat treatment consisting of bainite, retained austenite and spheroidal graphite.

The aim of this work is to show radical change in the design of the shaft, when experimentally determined values of fatigue strength in gigacycle region are applied in the mechanical design.

2 Experiments

ADI cast iron (Austempered ductile iron) was used as an experimental material in this study. ADI cast iron represents a typical material for shaft fabrication in automotive industry. The chemical analysis was made by the emission spectrometry method on ICP (JPY 385) emission spectrometer using fast recording system IMAGE. Chemical composition is shown in the Table 1. Experimental material was casted and then heat treated. This treatment consists of heating to the 910°C/30min for austenitization, followed by rapid cooling to tempering temperature 380°C and hold 60 minutes for isothermal transformation of austenite to bainite. Microstructure of testing materials after heat treatment is shown on the fig.1. and this is formed by bainite matrix, spheroidal graphite and small amount of retained austenite. Basic mechanical properties of the tested ADI cast iron after heat treatment are listed in the table 1. The tensile tests were carried out on a ZWICK Z050 testing machine at an ambient temperature 20±5°C, with the loading range in interval F=0÷20kN and the initial strain rate was $\varepsilon_m = 10^{-3}\ s^{-1}$. Round cross-section specimens were used, the shape and dimensions of the test specimens fulfilled the requirements of EN 10002-1 standard and five specimens were used for the tensile tests.

Fatigue tests were carried out on the high-frequency ultrasonic fatigue testing machine (Fig. 2), with working frequency 20 kHz. Using of high-frequency testing machines in tests in very-high cycle region is necessity, because achieving the required number of cycles by conventional testing machines (with working frequency f=50Hz) would take 231 days in comparison with 13.8 hours when high-frequency testing machines are used.

Table 1 Chemical composition and basic mechanical properties of ADI cast iron used in this study

	C	Mn	Si	P
wt. %	3.57	0.97	2.72	0.05
	S	Cu	Ni	Mo
wt. %	0.022	0.93	0.74	0.037
UTS [MPa]		YS [MPa]		Elongation [%]
1043		867		2.8

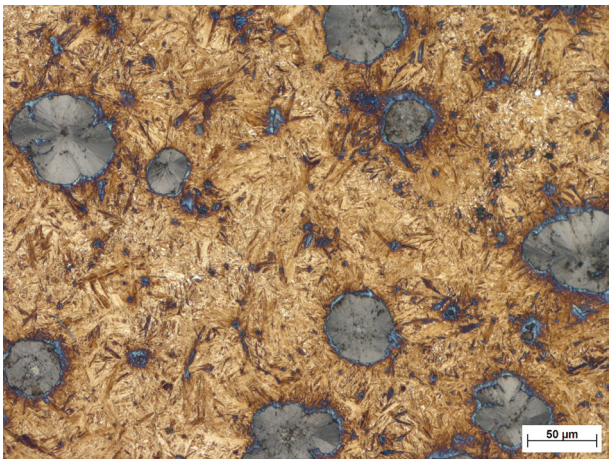

Fig. 1 Microstructure of ADI cast iron

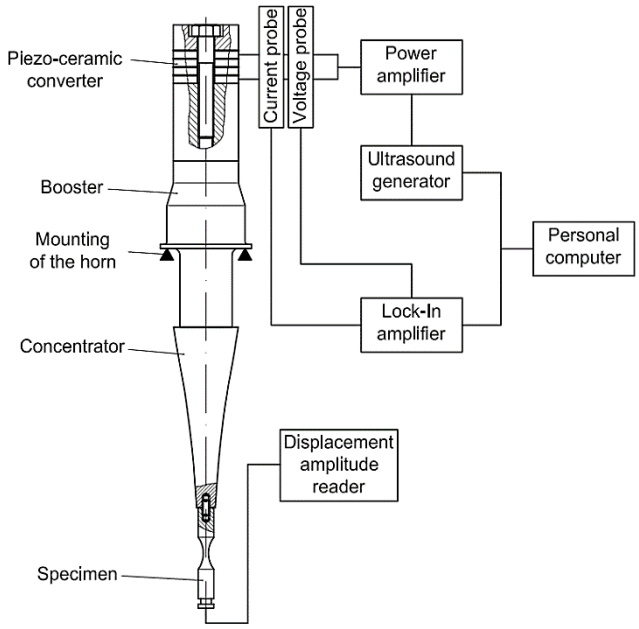

Fig. 2 Ultrasonic fatigue testing device for fatigue tests at f=20kHz

Specimens for the fatigue test were machined from the castings fulfilling the resonance conditions. Surface of specimens was grinded and polished to eliminate influence of machining on the fatigue tests results. Specimens were loaded by symmetrical push-pull loading (R=-1), with the frequency f=20 kHz and at the temperature 20±5°C. During whole test, specimens were submerged in water with anti-corrosive inhibitor to remove heat evolved during the test. From the tests results was constructed S-N curve (Fig. 3) and results were approximated by the Basquin equation:

$$\sigma_a = \sigma'_f \left(N_f\right)^b \tag{1}$$

to obtain dependence of the number of cycles to failure N_f on the loading stress amplitude, where b is exponent of fatigue live curve and σ'_f is the coefficient of fatigue strength σ_a obtained by extrapolation of stress amplitude σ_a on the first loading cycle (Skočovský, 2006; Bokůvka, 2015; Kohout, 2001). In the Table 2 are shown the values of conventional fatigue limit σ_c (evaluated for 10^7 cycles) and the fatigue limit σ_c for 10^9 cycles obtained from the S-N curve. Comparison of these values shows difference in the fatigue limits $\Delta\sigma_c$ approximately 290 MPa, what represents 67% reduction of fatigue strength.

Table 2 Comparison of fatigue limits for 10^7 and 10^9 cycles

σ_{c10^7}	σ_{c10^9}
430	140

3 Mechanical design of a shaft for different fatigue limits

Examples of the differences in mechanical design of a shaft when different operational lifetimes are considered will be given for a gearbox shaft with frontal (Z2) and conic (Z3) gears (Fig. 4). The shaft is loaded by a torque moment

$M_{tmax} = 6915.61\ Nm$, which represents the highest loading value. However, the short-time overload of the shaft might be present at the machine start-up, but this loading is usually just in the area of low-cycle fatigue and that is why it is not considered in this example of the shaft design for the high and the ultra-high cycle fatigue.

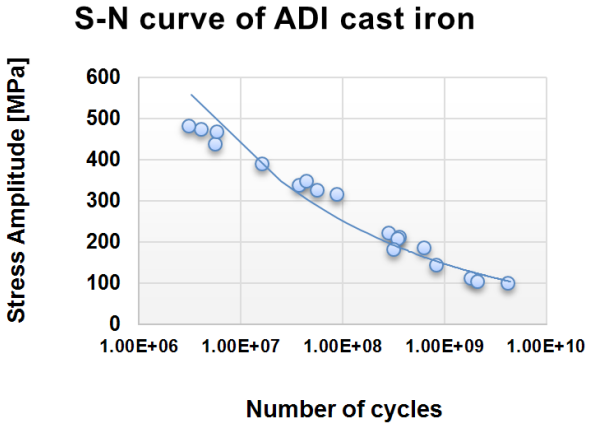

Fig. 3 S-N curve of ADI cast iron

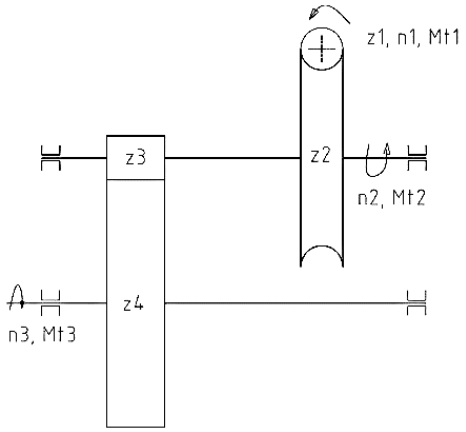

Fig. 4 Sketch of the gearbox; the analysed shaft with gears is marked by darker lines

3.1 Verification of static safety of the shaft

Firstly, it is necessary to analyse the values of loading forces on the axial (2), radial (3) and tangential (circumferential) (4) components:

$$F_{a2} = \frac{2 \cdot M_{t1}}{d_1} = -F_{t1} \tag{2}$$

$$F_{r2} = \frac{F_{t1} \cdot \tan \alpha_n}{\sin(\gamma + \varphi)} = F_{r1} \tag{3}$$

$$F_{t2} = \frac{2 \cdot M_{t2}}{d_2} = -F_{a1} \tag{4}$$

where F is the force (N), M_t is the torque moment (Nm), α is the pressure angle of the gear teeth (angle of obliquity) (20°), γ is the helix angle of the screw gear (16.6992°), φ is friction angle (0.7371°) and d is the mean value of the pitch diameter (Bolek, 1989; Bolek, 1990). Results of the force components, graphically shown in Fig. 5, are as follows:

Tangential forces:

$$F_{t12} = \frac{2 \cdot M_{t2}}{d_2} = \frac{2 \cdot 6915.61}{0.274} = 50467N \tag{5}$$

$$F_{t43} = \frac{2 \cdot M_{t2}}{d_3} = \frac{2 \cdot 6915.61}{0.17} = 81360N \tag{6}$$

Radial forces:

$$F_{r12} = \frac{F_{t1} \cdot \tan \alpha_n}{\sin(\gamma + \varphi)} = \frac{16019 \cdot \tan 20}{\sin(16.6992 + 0.7371)} = 19458N \tag{7}$$

$$F_{r43} = F_{t43} \cdot \tan \propto = 81360 \cdot \tan 20° = 29612N \tag{8}$$

Axial forces:

$$F_{a12} = \frac{2 \cdot M_{t1}}{d_1} = \frac{2 \cdot 1045.33}{0.13} = 16019N \tag{9}$$

$$F_{a43} = 0 \tag{10}$$

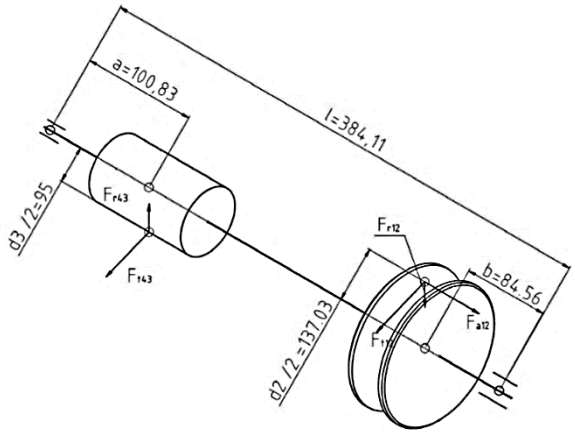

Fig. 5 Sketch for the analysis of the axial (F_a), radial (F_r) and tangential (F_t) components of the loading forces

Since the loading forces F_t, F_r and F_a are not oriented in the same plane, it is necessary to analyze the bending moments in two perpendicular planes, x - z and y - z (Fig. 6). The resulting bending moments are obtained by the vector sum of the partial bending moments (Fig. 7). To analyse the stress in the shaft, it is necessary to consider loadings in the points 1-5 (marked in Figs. 6 and 7). Table 3 shows the values of the bending stress (11), shear stress (12) and von Mises stress (13) which are obtained using the following equations:

$$\sigma_{bi} = \frac{M_{bi}}{W_{bi}} \tag{11}$$

$$\tau_{ti} = \frac{M_{ti}}{W_{ti}} \tag{12}$$

$$\sigma_{vM} = \sqrt{\sigma_{bi}^2 + 3 \cdot \tau_{ti}^2} \tag{13}$$

where σ_{bi} is the bending stress (Pa), τ_{ti} is the shear stress (Pa), σ_{vM} is the von Mises stress, M_b is the bending moment (Nm), W_b is the bending section modulus (m^3), M_t is the torque moment (Nm), W_t is the torque section modulus (m^3) (Várkolyová, 2006; Kohár, 2006).

Table 3 Resulting bending and torque moments in points 1-5

Point *i*	1	2	3	4	5
Bending moment M_{bi} *(Nm)*	436.3	1932.7	6669.3	5918.0	1756.5
Torque moment M_{ti} *(Nm)*	0	0	6914.9	6914.9	0
Bending stress σ_{bi} *(MPa)*	5.2	16.1	29.5	56.8	20.9
Shear stress τ_{ti} *(MPa)*	0	0	15.3	33.2	0
von Mises stress σ_{vM} *(MPa)*	5.2	16.1	39.7	80.8	20.9

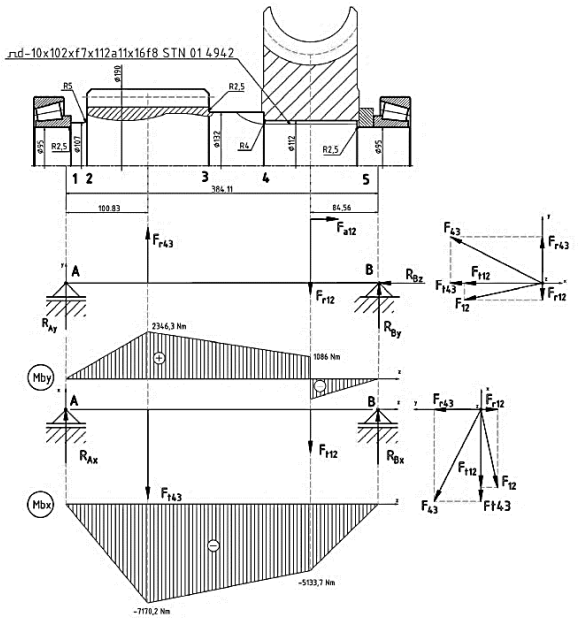

Fig. 6 Partial bending moments in two perpendicular planes x-z and y-z

In Table 3 one can see that the highest value of von Mises stress (σ_{vM}) is in the point 4 (Fig. 7), which means that this point is subjected to the highest load; therefore, this is a critical region of the shaft. The value of the static safety coefficient is evaluated according to Eq. (14):

$$k_s = \frac{R_{p02}}{\sigma_{vM4}} = \frac{867}{80.8} = 10.73 \tag{14}$$

where k_s is the static safety coefficient, R_{p02} is the proof stress (Pa) and σ_{vM4} is the von Mises stress in the point 4 (Pa). The value of the resulting static safety coefficient is very high, which results in high safety in terms of static loading and which assumes that the shaft is over equipped. However, a determining factor for safe operation is the cyclic loading; therefore, it is necessary to verify the shaft in terms of fatigue lifetime.

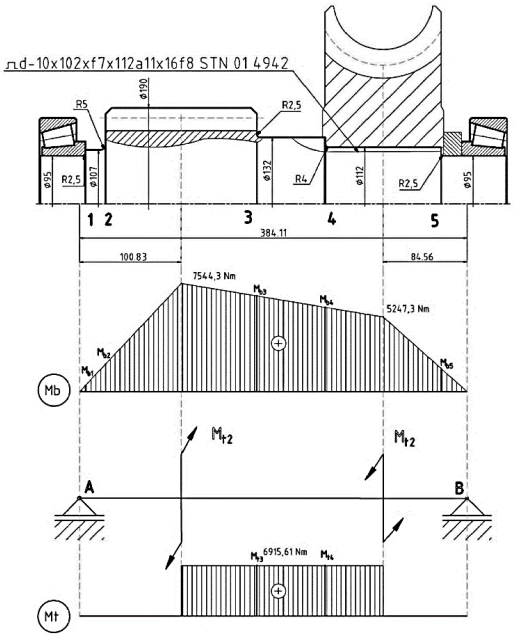

Fig. 7 Resulting bending and torque moments in the analysed shaft

3.2 Verification of fatigue safety of the shaft

The shaft fatigue safety will be verified in the points 2 and 4 (Fig. 7) where the highest static loadings and also notches are present. The example of verification of point 4 is drawn in detail and the results for both verified points are given in Table 4. To compare the differences in the shaft size, the shaft safety will be verified with respect to the fatigue strength in the regions of high-cycle fatigue ($N = 10^7$ cycles) and of ultra-high-cycle fatigue ($N = 10^9$ cycles).

As the shaft is fitted into bearings so that it can turn, the forces created by meshing gears are not changing. Hence, it can be considered that the shaft is loaded by symmetrical bending cyclic loading, with a cycle asymmetry ratio of R = -1 (Fig. 8a). For the torsional fatigue loading, the discrete loading in operation is considered; therefore, the shaft will be loaded by a disappearing cycle, with a cycle asymmetry ratio of $R = 0$ (Fig. 8b).

3.2.1 Bending loading (point 4)

Fatigue limit of ADI cast iron for $N = 10^7$ cycles, tested on small (diameter of 4 mm), polished (R_a = 0.4 μm) specimens (Table 4), is $\sigma_{bc} = 430\ MPa$. To consider the stress concentration caused by the notch (diameter change on the shaft), the fatigue limit has to be modified according to Eq. (15):

$$\sigma_{bc}^{*} = \frac{\sigma_{bc} \cdot \upsilon_{\sigma} \cdot \varepsilon_{s}}{\beta_{\sigma}} = \frac{430 \cdot 0.73 \cdot 0.875}{2.44} = 112.6 MPa \quad (15)$$

where σ_{bc}^{*} is the modified fatigue limit, υ_{σ} is the size factor (for the alloyed steel specimen with a diameter of 102 mm, its value is 0.73 (Shigley, 2010; Leinveber, 2006)), ε_{s} is the surface factor (for tensile strength R_{m} = 1043 *MPa*, its value is 0.875 (Shigley, 2010; Leinveber, 2006) and β_{σ} is the notch concentration factor, calculated by FEA (Fig. 9), because in the point 4 there are combined two notch concentrators (diameter change and the grooves on the shaft) and that kind of combined notch concentrator (β_{σ}) is not included in any normograms.

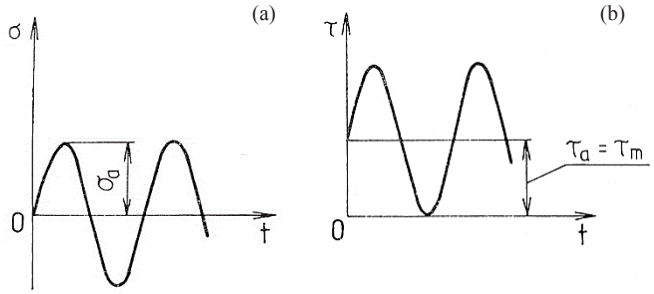

Fig. 8 Types of shaft fatigue loading: bending loading (left – Fig. 8a) and torque loading (right – Fig. 8b)

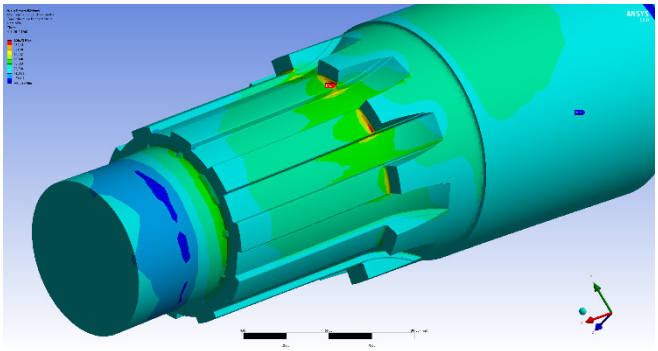

Fig. 9 FEA for determining the notch concentrator factor β_{σ}

Bending loading amplitude in the point 4.

$$\sigma_{ba} = \sigma_{b4} = 56.8 MPa \quad (16)$$

To fulfil the safety requirements, the value of dynamic safety factor (17) must be higher than 1.3 ($k_{\sigma} \geq k_{min}$ = 1.3 (Málik, 2003)).

$$k_{\sigma 4} = \frac{\sigma_{bc}^{*}}{\sigma_{b4}} = \frac{112.6}{56.8} = 1.983 > k_{\min} = 1.3 \rightarrow accomplished \quad (17)$$

3.2.2 Torque loading (point 4)

Fatigue limit for the torque loading of ADI cast iron evaluated for $N = 10^{7}$ cycles is:

$$\tau_{tc} = 0.57 \cdot \sigma_{bc} = 0.57 \cdot 430 = 245.1 MPa \quad (18)$$

However, this value is obtained from the fatigue limit determined by fatigue tests carried out at R = -1 and the torque loading is considered as R = 0. This means that the safety verification according to Eq. (21) must be done using a coefficient of the material sensitivity to the loading cycle asymmetry ψ_{τ}, which covers a potential difference in the fatigue limits obtained at different cycle asymmetry ratios.

Fatigue limit for torque loading when the notch is considered:

$$\tau_{tc}^{*} = \frac{\tau_{tc} \cdot \upsilon_{\sigma} \cdot \varepsilon_{s}}{\beta_{\tau}} = \frac{245.1 \cdot 0.73 \cdot 0.875}{2.02} = 77.5 MPa \quad (19)$$

where τ_{tc}^{*} is the modified fatigue limit, υ_{σ} is the size factor (for the alloyed steel specimen with a diameter of 102 mm, its value is 0.73 (Shigley, 2010; Leinveber, 2006)), ε_{s} is the surface factor (for tensile strength R_{m} = 1043 *MPa*, its value is 0.875 (Shigley, 2010; Leinveber, 2006)) and β_{τ} is the notch concentration factor in the root of the equilateral groove, which was determined by the FEA, according to the Fig. 10 (for internal radius 0.5 mm, its value is 2.02).

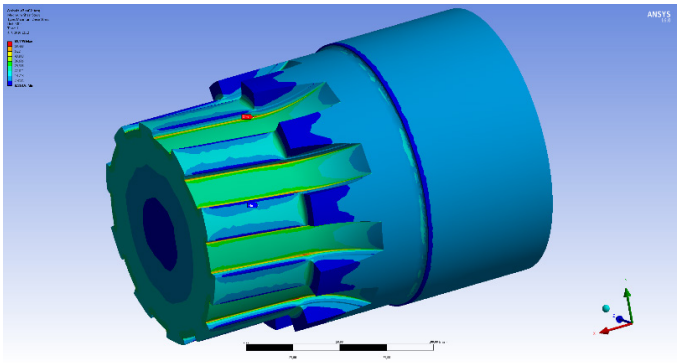

Fig. 10 FEA for determining the notch concentrator factor β_{τ}

Torque loading amplitude and a mean stress (according a Fig. 7) value in the point 4 is expressed as:

$$\tau_{ta} = \tau_{tm} = \frac{\tau_{t4}}{2} = \frac{33.2}{2} = 16.6 MPa \quad (20)$$

where τ_{t4} is the maximal shear stress in the point 4 (Table 3). Again, in order to fulfil the safety requirements, the value of dynamic safety factor (21) must be higher than 1.3 ($k_{\tau} \geq k_{min}$ = 1.3 (Málik, 2003)).

$$k_{\tau 4} = \frac{\tau_{tc}^{*} - \psi_{\tau} \cdot \tau_{tm}}{\tau_{ta}} = \frac{77.5 - 0.05 \cdot 16.6}{16.6} = 4.62 > k_{\min} = 1.3 \rightarrow accomplished \quad (21)$$

where τ_{ta} is the torque loading amplitude, τ_{tm} is the mean shear stress, ψ_{τ} is the factor representing the material sensitivity to the loading cycle asymmetry (for shear stress and UTS, it is ψ_{τ} = 0.05 (Málik, 2003)).

3.2.3 The total safety coefficient under the action of shear and normal stresses (point 4) (22):

$$k_{red} = \frac{k_\sigma \cdot k_\tau}{\sqrt{k_\sigma^2 + k_\tau^2}} = \frac{1.983 \cdot 4.62}{\sqrt{1.983 + 4.62}} = 1.82 \rightarrow accomplished \quad (22)$$

where k_σ represents the dynamic safety factor for normal stress and k_τ represents the dynamic safety factor for tangential stress.

The results given in Table 4 show that the points 4 fulfil the condition for dynamic safety k_{red} for $N = 10^7$ cycles, but not for $N = 10^9$. To satisfy the condition of dynamic safety for the shaft, it is necessary to make adjustments in the shaft design. Influence of radius between the shaft's steps in the point 4 on the safety coefficients k_σ and k_{red} is shown in the tab.4. In the point 4, the shaft diameters should be increased from 112 mm to 120 mm and also the size of the splining according to Fig. 11.

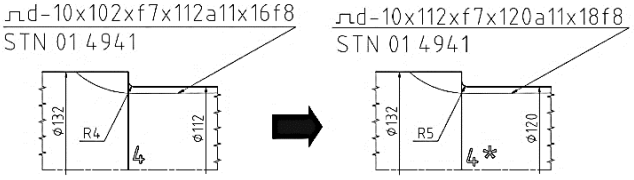

Fig. 11 Adjustment in the shaft design in point 4

After adjustments in the shaft design have been made, it is necessary to verify the shaft dynamic safety once again. The verified points of the shaft after the design adjustments are marked as 4* and the results are given in Table 5 together with a comparison with the results of the point 4 (before design adjustment). After the dimensional changes, the shaft fulfils the condition for dynamic safety for $N = 10^9$ cycles. Fig. 12 shows effect of shaft modification on the total safety coefficient k_{red} depending on the size of radius between the shaft's steps.

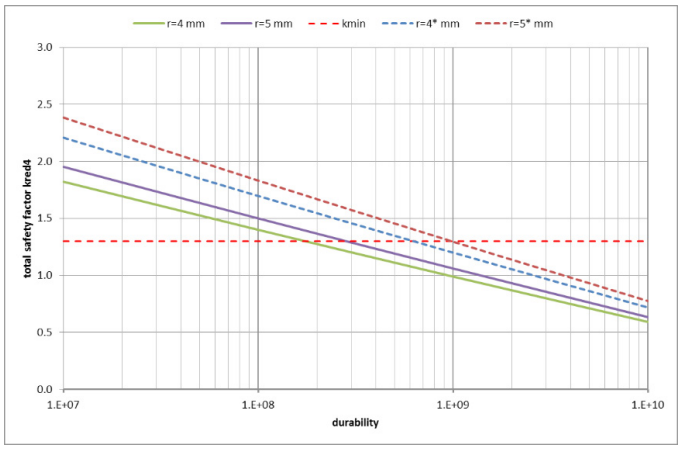

Fig. 12 Dependence of total safety coefficient on the size of radius between the shaft's steps in the point 4 (with and without adjustment of design)

Table 4 Results of loading stress and the safety coefficients for points 4 of the shaft when fatigue strengths for **N = 10⁷** cycles and **N = 10⁹** cycles are considered

Number of cycles Nf	Radius R1 (mm)	Bending					Torque					Safety coefficient	Safety condition
		β_σ	σ_c (MPa)	σ_{bc}^* (MPa)	σ_{b4} (MPa)	k_σ	β_τ	τ_t (MPa)	τ_{tc}^* (MPa)	τ_{t4} (MPa)	k_τ	k_{red}	$k_\sigma, k_\tau, k_{red} \geq k_{min} = 1.3$
10^7	2	2.928	430	93.9	56.8	1.653	2.023	245.1	77.5	16.6	4.619	1.556	accomplished
	3	2.611		105.3		1.854						1.720	accomplished
	4	2.441		112.6		1.983						1.822	accomplished
	5	2.246		122.4		2.155						1.953	accomplished
10^9	2	2.928	233.7	51.0	56.8	0.899	2.023	133.2	42.1	16.6	2.488	0.845	failed
	3	2.611		57.2		1.008						0.934	failed
	4	2.441		61.2		1.078						0.989	failed
	5	2.246		66.5		1.171						1.060	failed

Table 5 Results of loading stress and the safety coefficients after design adjustments for point 4* compared to the ones calculated for point 4 (before adjustments)

Number of cycles Nf	Point i	Radius R1 (mm)	Bending					Torque					Safety coefficient	Safety condition	Shaft weight
			β_σ	σ_c (MPa)	σ_{bc}^* (MPa)	σ_{b4} (MPa)	k_σ	β_τ	τ_t (MPa)	τ_{tc}^* (MPa)	τ_{t4} (MPa)	k_τ	k_{red}	$k_\sigma, k_\tau, k_{red} \geq k_{min} = 1.3$	m (kg)
10^9	4	4	2.441	233.7	61.2	56.8	1.078	2.023	133.2	42.1	16.6	2.488	0.989	failed	41.63
10^9	4*	2	3.119	233.7	47.2	42.91	1.100	2.032	245.1	41.3	12.5	3.245	1.042	failed	43.98
		3	2.778		53.0		1.235						1.155	failed	
		4	2.659		55.4		1.291						1.199	failed	
		5	2.43		60.6		1.412						1.30	accomplished	

4 Results and discussion

Advances in the engineering in the recent few decades caused that conventional fatigue limit (given for the number of cycles 10^7) cannot be satisfying for the many todays applications, as it was proven by many authors, that failure of engineering materials can occur after higher numbers of cycles than conventional number of loading cycles (10^7) and the behaviour of materials in the ultra-high cycle region is different, depending on the particular type of the material. High frequency fatigue testing of ADI cast iron shows, that in this material, failure can occur even after 10^7 cycles, a standard fatigue limit. There was recorded significant decrease of fatigue strength in the ultra-high cycle region. This behaviour was observed for many structural materials, and it just confirm the observation of other authors about failure of structural elements caused by cyclic loading lower than the conventional fatigue limit (Trško, 2016; Nový, 2011; Stanzl, 1999; Bathias, 1999). The difference between fatigue strength for 10^7 and 10^9 numbers of loading cycles was $\Delta\sigma_c$=290*MPa,* what is reduction of fatigue strength by 67%.

According to aforementioned facts, in mechanical design of shaft for cyclic loading in ultra-high cycle region is necessary applied the values of fatigue strength for 10^9 cycles instead conventional value for the 10^7 cycles. Dramatic decrease of fatigue strength must be reflected to the mechanical design, to fulfil the safety conditions for shaft design. The most critical part of the designed shaft are notches, in which during cyclic loading local stress amplitude reaches a critical value. To meet the safety requirements in necessary to adjust a geometry in these notches parts and increase the size and diameter of the most stressed parts, what can result in some increase of the weight of structural component.

5 Conclusions

Based on the carried out fatigue tests and applying its results to the shaft design can be stated following conclusions:

- Failure of ADI cast iron can occur even after conventional fatigue limit (10^7 cycles)
- High frequency fatigue test of ADI cast iron show continuously decrease of fatigue strength in the ultra-high cycle region
- The difference between fatigue strength of ADI cast iron at 10^7 and 10^9 cycles was $\Delta\sigma_c$ = 290MPa, what is a 67% reduction of fatigue strength
- The reduction of fatigue strength significantly affects the mechanical design of shaft, especially in notches, where to fulfil the safety requirements, it is necessary to adjust the design of these highly stressed elements to decrease the notch effect or increase the size of loaded components to reduces the stress values
- Introduction of the fatigue strength values for 10^9 cycles cause the increase of the weight of structural component by 5.6%.

Acknowledgement

The research is supported by Scientific Grant Agency of the Ministry of Education, Science, Research and Sport of the Slovak Republic under the contract VEGA no. 1/0396/14 and VEGA no. 1/0123/15.

References

Bathias, C. (1999). There Is No Infinite Fatigue Life in Metallic Materials. *Fatigue & Fracture of Engineering Materials & Structures*. 22(7), pp. 559–565. https://doi.org/10.1046/j.1460-2695.1999.00183.x

Bokůvka, O., Nicoletto, G., Guagliano, M., Kunz, L., Palček, P., Nový, F. (2015). *Fatigue of Materials at Low High Frequency Loading.* EDIS ZU, Žilina, Slovakia.

Bolek, A., Kochman, J., et al. (1989). *Časti strojů 1. svazek*. (Machine parts 1. volume). SNTL Praha, (in Czech).

Bolek, A., Kochman, J., et al. (1990). *Časti strojů 2. svazek*. (Machine parts 2. volume). SNTL Praha, (in Czech).

Filo, M., Málik, L., Čillík, L., Žiačik, A., Barysz, I., Kraus, V. (1990). *Časti a mechanizmy strojov, príklady*. (Parts and machine mechanisms, examples.) ALFA, Bratislava, (in Slovak).

Kohár, R., Ságа, M., Vaško, M., Kocúr, R., Toth, Ľ. (2006). *Aplikácia optimalizačných algoritmov v mechanike telies (Application of optimization algorithms in the mechanics of bodies).* VTS Žilina, (in Slovak).

Kohout, J.,Věchet, S. (2001). A new function for fatigue curves characterization and its multiple merits. *International Journal of Fatigue*. 23, pp. 175-183. https://doi.org/10.1016/S0142-1123(00)00082-7

Leinveber, J., Vávra, P. (2006). *Strojnické tabulky*. (Handbook of mechanical engineering.) ALBRA, Úvaly. (in Czech).

Málik, L., Medvecký, Š., Brumerčík, F., Hrček, S., Chrzová, J., Kohár, R. (2003). *Časti a mechanizmy strojov*. (Parts and machine mechanisms.) EDIS ŽU, Žilina. (in Slovak).

Murakami, Y. (2002). *Metal Fatigue: Effects of Small Defects and Nonmetallic Inclusions.* 1st ed., Elsevier, Oxford.

Nový, F., Bokůvka, O., Mintách, R., Trško, L. (2011). Influence of steels strength on the ultra-high cycle fatigue lifetime. *Perner's Contacts*. 6(2), pp. 131-135.

Ritchie, R. O., Davidson, D. L., Boyce, B. L., Campbell, J. P., Roder, O. (1999). High-Cycle Fatigue of Ti-6A1-4V. *Fatigue & Fracture of Engineering Materials & Structures*. 22(7), pp. 621–631. https://doi.org/10.1046/j.1460-2695.1999.00194.x

Shigley, J. E., Mischke, Ch. R., Budynas, R. G. (2010). *Konstruování strojních součástí*. (Design of machine parts.) Nakladatelství VUTIUM. (in Czech)

Skočovský, P., Bokůvka, O., Konečná, R., Tillová, E. (2006). *Náuka o materiáli pre odbory strojnícke.* (Material science for students of mechanical engineering.) EDIS ŽU, Žilina, (in Slovak).

Stanzl-Tschegg, S. E. (1999).Fracture mechanisms and fracture mechanics at ultrasonic frequencies. *Fatigue & Fracture of Engineering Materials & Structures*. 22(7), pp. 567–579. https://doi.org/10.1046/j.1460-2695.1999.00180.x

Trško, L., Bokůvka, O., Nový, F., Lago, J. (2016). Quality and fatigue characteristics relation. *Production Engineering Archives*. 10(1), pp. 9-12.

Várkolyová, B., Dekýš, V., Toth, Ľ. (2006). *Pružnosť a pevnosť I.* (Advanced strength and applied elasticity I.) VTS Žilina. (in Slovak).